Emergent orbitals in the cluster Mott insulator on a breathing kagome lattice

Emergent orbitals in the cluster Mott insulator on a breathing kagome lattice

Gang Chen*
Department of Physics, Center for Field Theory and Particle Physics, State Key Laboratory of Surface Physics, Fudan University, Shanghai 200433, China
and Collaborative Innovation Center of Advanced Microstructures, Nanjing 210093, China

Patrick A. Lee
Department of Physics, Massachusetts Institute of Technology, Cambridge, Massachusetts 02139, USA

(Received 30 September 2017; published 12 January 2018)

Motivated by the recent developments on cluster Mott insulating materials such as the cluster magnet $LiZn_2Mo_3O_8$, we consider the strong plaquette charge ordered regime of the extended Hubbard model on a breathing kagome lattice and reveal the properties of the cluster Mottness. The plaquette charge order arises from the intersite charge interaction and the collective motion of three localized electrons on the hexagon plaquettes. This model leads naturally to a reduction of the local moments by $2/3$, as observed in $LiZn_2Mo_3O_8$. Furthermore, at low temperatures, each hexagon plaquette contains an extra orbital-like degree of freedom in addition to the remaining spin $1/2$. We explore the consequence of this emergent orbital degree of freedom. We point out the interaction between the local moments is naturally described by a Kugel-Khomskii spin-orbital model. We develop a parton approach and suggest a spin-liquid ground state with spinon Fermi surfaces for this model. We further predict an emergent orbital order when the system is under a strong magnetic field. Various experimental consequences for $LiZn_2Mo_3O_8$ are discussed, including an argument that the charge ordering must be short ranged if the charge per Mo is slightly off stoichiometric.

DOI: 10.1103/PhysRevB.97.035124

I. INTRODUCTION

Spin, charge, and orbital are three basic degrees of freedom of condensed matter systems, and their mutual interaction, interplay, and entanglement cover the major topics of modern condensed matter physics [1–4]. In conventional Mott insulators, electron charge localization creates local spin moments at the lattice sites, and the orbital degree of freedom becomes active when the local crystal symmetry allows the degeneracy of atomic orbitals [3]. Recently, the cluster Mott insulator has emerged as a new type of Mott insulator in which the electrons are localized inside the cluster [5–13]. As a result, the keen interplay between the charge and the spin degrees of freedom in cluster Mott insulators (CMIs) is often quite different from a conventional Mott insulator [5–8]. In particular, it was shown that the two-dimensional CMIs of the kagome system [6,8] with an extended Hubbard model at $1/6$ electron filling may develop a plaquette charge order [14–18] on hexagon plaquettes (see Fig. 1). This plaquette charge order immediately impacts the spin degree of freedom and modulates the spin properties by reconstructing the spin state within each plaquette. Such a charge-driven spin-state reconstruction is one crucial property of the CMIs in this system [6].

Well-known examples of cluster magnets include $LiZn_2Mo_3O_8$, $Li_2InMo_3O_8$ [19], and $ScZnMo_3O_8$ [20], where the Mo electrons are in the CMIs with the Mo electrons localized in the smaller triangular clusters of the distorted kagome lattice (see Fig. 1) [21–25]. The distortion is such that the up and down triangles have different bond lengths and the lattice is often referred to as the breathing kagome. Interestingly, the material $LiZn_2Mo_3O_8$ experiences two Curie regimes with distinct Curie-Weiss temperatures and Curie constants [22,23] in which the low-temperature Curie constant is $1/3$ of the high-temperature one and the low-temperature Curie-Weiss temperature is much smaller than the high-temperature one. Moreover, the system remains magnetically disordered down to the lowest measured temperature, and inelastic neutron scattering does observe

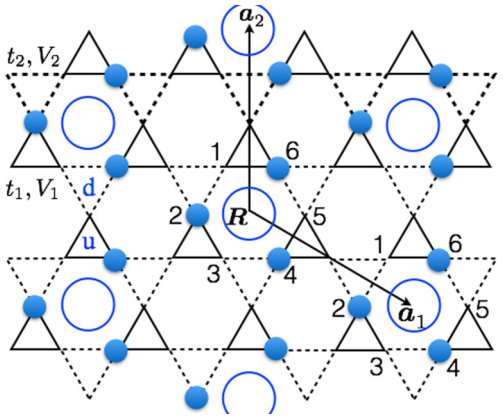

FIG. 1. The breathing kagome lattice with plaquette charge order. The solid (dashed) lines represent the up (down) triangles. The plaquette charge order hosts three electrons that are resonating on hexagons with circles marked, and $\boldsymbol{a}_1$,$\boldsymbol{a}_2$ are two lattice vectors that connect neighboring resonating hexagons. $\boldsymbol{R}$ labels the resonating hexagon, and 1–6 label the six vertices.

*gangchen.physics@gmail.com

a continuum of excitations [21]. This is consistent with the proposal of a spin-liquid ground state in this material. Partly inspired by the experiments in $LiZn_2Mo_3O_8$, we here explore the strong plaquette charge ordered regime of the CMI on the breathing kagome system where the electron charges are localized on resonating hexagon plaquettes (see Fig. 1). In addition to the on-site repulsion, a large intersite repulsion is assumed which forbids the occupation of neighboring sites. This leads to plaquette charge ordering and the expansion of the unit cell, formed by a triangular lattice of hexagons marked by the circles in Fig 1. The low-lying degree of freedom is the collective resonant rotation of the three occupied sites on each hexagon (see Fig. 2). To put this model in the context of the earlier model by Flint and Lee [26], there the intersite repulsion is assumed to be weak and each up triangle is occupied by one electron, and no correlation is assumed around the hexagons. The up triangles form a triangular lattice and a lattice distortion is postulated which creates a honeycomb lattice of up triangles, with the spin at the center of the honeycomb relatively isolated and responsible for the local moments at low temperatures. Note that both for this model and the current model, a tripling of the unit cell is assumed. This has been searched for by x-ray scattering but so far no new diffraction peaks have been observed. This issue will be discussed in the Discussion section, where we point out that if the system is slightly off stoichiometric, domain walls will form between the ordered states. Due to a special feature of domain walls forming a honeycomb lattice [27], it can be shown that long-range order is always destroyed, i.e., the system can only have short-range order. This may help explain the absence of new diffraction spots, and both models may remain viable. We also point out that the Flint-Lee model addressed only the freeze-out of 2/3 of the spins at low temperatures, and the ultimate fate of the local moments that remained was not discussed. In the current model, we address both the freeze-out and the true ground state of this system and argue that due to an emergent orbital degree of freedom, a spin-liquid state may form as the true ground state.

We also compare the current paper with a previous work on a similar model [6] which treats the weak plaquette order regime. The current treatment of the CMI is analogous to the strong Mott regime of a conventional Mott insulator, while the previous weak plaquette charge ordered regime [6] is similar to the weak Mott regime (i.e., close to the Mott transition) where the charge fluctuation may destabilize the spin order and lead to a spin liquid [28,29]. We find that in the strong charge ordered regime, the charge-spin interaction appears in a much more straightforward and transparent manner. We explain the local moment reconstruction in the presence of a strong plaquette charge order on the hexagon, giving rise to a net spin-1/2 local moment on the hexagon. We point out that there exists an emergent orbital-like degree of freedom. These emergent orbitals are twofold degenerate and protected by the symmetry of the hexagon plaquette. The natural model that describes the interaction between the effective spin and the emergent orbital on the hexagon plaquette is the Kugel-Khomskii exchange model [30]. As a comparison with conventional Mott insulators, the Kugel-Khomskii model is used to describe the exchange interaction between the local moments when an orbital degeneracy exists for the atomic orbitals [30].

For the Kugel-Khomskii model, we design a fermionic parton approach to represent the effective spin and the emergent orbital degrees of freedom, and propose a spinon Fermi-surface spin-liquid ground state. We point out that the emergent orbital generically creates nondegenerate spinon bands and allows interband particle-hole excitations. Specifically, the interband particle-hole excitations would manifest as a finite-energy spinon continuum at the Γ point in inelastic neutron scattering and optical measurements. Polarizing the spin degrees of freedom by applying strong magnetic fields, we obtain a simple 120° compass model for the emergent orbital interaction. We further predict that the system selects a specific orbital order via order by quantum disorder and supports a nearly gapless pseudo-Goldstone mode. These results establish a different perspective on the Mottness of the CMI.

The paper is organized as follows. In Sec. II, we introduce the extended Hubbard model and explain the plaquette charge order. In Sec. III, we explain the local moment structure of the resonating hexagon in the strong plaquette charge ordered regime and point out the fundamental existence of the emergent orbital degree of freedom. In Sec. IV, we derive the Kugel-Khomskii model that describes the exchange interaction between the spin and the orbital on the triangular lattice formed by the resonating hexagons. In Sec. V, we design a parton construction and suggest the features of the spinon continuum for the proposed spinon Fermi-surface ground state. In Sec. VI, we explain the emergent orbital order, quantum order by disorder effect of the compass model for the orbitals, and the orbital excitation when the spin is polarized by an external magnetic field. In Sec. VII, we discuss the relevance of this model to $LiZn_2Mo_3O_8$ and explore various experimental consequences. We end with a broad view on the cluster Mott insulating materials.

II. THE MICROSCOPIC MODEL AND THE PLAQUETTE CHARGE ORDER

We start with the extended Hubbard model on the breathing kagome lattice (see Fig. 1),

$$H = -\sum_{\langle ij\rangle\in \mathrm{u}} (t_1 c^\dagger_{i\sigma} c_{j\sigma} + \mathrm{H.c.}) - \sum_{\langle ij\rangle\in \mathrm{d}} (t_2 c^\dagger_{i\sigma} c_{j\sigma} + \mathrm{H.c.}) + \sum_{\langle ij\rangle\in \mathrm{u}} V_1 n_i n_j + \sum_{\langle ij\rangle\in \mathrm{d}} V_2 n_i n_j + \sum_i U n_{i\uparrow} n_{i\downarrow}, \quad (1)$$

where $c^\dagger_{i\sigma}$ ($c_{i\sigma}$) creates (annihilates) an electron with spin σ ($=\uparrow,\downarrow$) at the lattice site i, n_i ($\equiv n_{i\uparrow}+n_{i\downarrow}$) is the electron occupation number, and "u" and "d" refer to the up and down triangles that are of different sizes, respectively. Here, t_1 and V_1 (t_2 and V_2) are the electron hopping and repulsion on neighboring sites of the up (down) triangles, respectively. The electron filling is 1/6, i.e., one electron per unit cell on the breathing kagome lattice. This model was suggested to capture the physics of Mo-based cluster magnets such as $LiZn_2Mo_3O_8$ in which the Mo atoms form a breathing kagome lattice [6,19,20].

The Hubbard U interaction for our system merely removes the electron double occupancy on the lattice site, but it cannot localize the electrons on the lattice sites. The electrons can move on the lattice without encountering any double

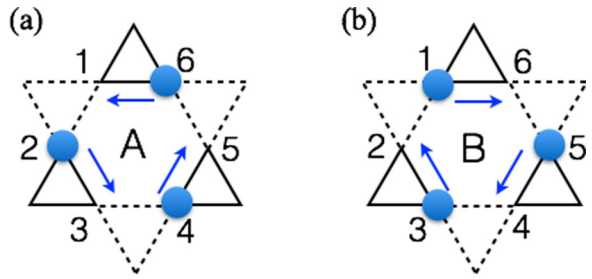

FIG. 2. The correlated and collective motion of the three electrons on the elementary hexagon. The arrow indicates the hopping direction. Note that the hoppings of the three electrons happen at the same time.

occupancy. This is quite different from a conventional Mott insulator where the electrons are localized on the lattice sites. It is the intersite interactions V_1 and V_2 that localize the electron on the triangular clusters of the kagome system. Despite being localized on the triangular clusters, the electrons manage to fluctuate in a collective fashion due to the extensive degeneracy of the electron occupation configuration on the kagome lattice. As U is often quite large compared to t_1, t_2, V_1, V_2, one could safely ignore the electron configurations with any double occupancy. With a third-order degenerate perturbation of the electron hoppings, we obtain an effective Hamiltonian that operates on the degenerate electron occupation manifold and is given as [6]

$$H_{\rm eff} = -\sum_{\hexagon}\sum_{\alpha\beta\gamma}[K_1(c^\dagger_{1\alpha}c_{6\alpha}c^\dagger_{5\beta}c_{4\beta}c^\dagger_{3\gamma}c_{2\gamma} + \text{H.c.}) + K_2(c^\dagger_{1\alpha}c_{2\alpha}c^\dagger_{3\beta}c_{4\beta}c^\dagger_{5\gamma}c_{6\gamma} + \text{H.c.})], \quad (2)$$

where we have

$$K_1 = 6t_1^3/V_2^2, \quad K_2 = 6t_2^3/V_1^2, \quad (3)$$

and "1, 2, 3, 4, 5, 6" refer to the six vertices on the elementary hexagon of the kagome lattice. $H_{\rm eff}$ describes the correlated and collective motion of the three electrons on the elementary hexagon (see Fig. 2). By mapping the electron occupation to the dimer covering on the dual honeycomb lattice [6,31], the previous work has obtained a plaquette charge order where the electrons preferentially occupy 1/3 of the hexagons in a periodic fashion (see Fig. 1) [6,14,16–18,32]. This plaquette charge order is a quantum effect because the three electrons are resonating on the hexagons and form a linear superposition of the two occupation configurations [6]. In the strong plaquette charge ordered limit, the electron (charge) occupation wave function would be well approximated by a simple product state with

$$|\Psi\rangle_{\rm c} = \prod_{\boldsymbol{R}} \frac{1}{\sqrt{2}}[|\hexagon_{\boldsymbol{R}}\rangle_{\rm A} + |\hexagon_{\boldsymbol{R}}\rangle_{\rm B}], \quad (4)$$

where $\boldsymbol{R}$ refers to the position of the resonating hexagons, and A and B label the two charge occupation configurations of the three electrons on the resonating hexagon (see Fig. 1). The spin quantum number can still be transferred via the spin exchange interaction, so $|\Psi\rangle_{\rm c}$ merely represents the charge wave function.

III. THE EMERGENT ORBITALS AND THE LOCAL MOMENTS

In this section, we focus on the strong plaquette charge ordered regime and reveal the different features of the local moment structure. The three electrons are well localized on the resonating hexagons but still move in a collective fashion that is governed by $H_{\rm eff}$. This collective motion tunnels the electron spins that are interacting with the superexchange interaction at the same time. As a comparison, the localized electrons on a lattice site of a conventional Mott insulator are fully governed by the atomic electron interactions and the Hund's rules. Here, the right model that describes the localized electrons on an individual resonating hexagon is

$$H_{\hexagon_{\boldsymbol{R}}} = -K_1\sum_{\alpha\beta\gamma}(c^\dagger_{1\alpha}c_{6\alpha}c^\dagger_{5\beta}c_{4\beta}c^\dagger_{3\gamma}c_{2\gamma} + \text{H.c.}) - K_2\sum_{\alpha\beta\gamma}(c^\dagger_{1\alpha}c_{2\alpha}c^\dagger_{3\beta}c_{4\beta}c^\dagger_{5\gamma}c_{6\gamma} + \text{H.c.}) + H_{\text{ex},\boldsymbol{R}}, \quad (5)$$

where the superexchange interaction is given as

$$H_{\text{ex},\boldsymbol{R}} = J\sum_{\langle\langle ij\rangle\rangle\in\hexagon_{\boldsymbol{R}}}\left(\mathbf{S}_i\cdot\mathbf{S}_j - \frac{1}{4}\right)n_i n_j. \quad (6)$$

It is interesting to note that the above superexchange differs from the usual form of the exchange interaction by having extra electron density operators n_i and n_j. This is because the positions of the electrons are not fixed due to their collective tunneling on the hexagon plaquette. The local Hilbert space of $H_{\hexagon_{\boldsymbol{R}}}$ also differs significantly from the on-site one for a conventional Mott insulator, and is instead spanned by the electron states that are labeled by both the positions and the spin quantum numbers of the three resonating electrons. Because the electrons are separated from each other by one lattice site due to the repulsive interaction, the Hilbert space for the electron positions is highly constrained. For the resonating hexagon centered at $\boldsymbol{R}$, there are in total 16 states that are labeled by

$$|\alpha\beta\gamma\rangle_{\rm A} \equiv |n_1=0\rangle|n_2=1,\alpha\rangle|n_3=0\rangle \times|n_4=1,\beta\rangle|n_5=0\rangle|n_6=1,\gamma\rangle, \quad (7)$$

$$|\alpha\beta\gamma\rangle_{\rm B} \equiv |n_1=1,\alpha\rangle|n_2=0\rangle|n_3=1,\beta\rangle \times|n_4=0\rangle|n_5=1,\gamma\rangle|n_6=0\rangle, \quad (8)$$

where $\alpha,\beta,\gamma\,(=\uparrow,\downarrow)$ refer to the electron spins at the occupied site. Since the hexagonal Hamiltonian $H_{\hexagon_{\boldsymbol{R}}}$ commutes with the total spin $\mathbf{S}_{\rm tot}$ and $S^z_{\rm tot}$ of the three resonating electrons, we use $\{S_{\rm tot}, S^z_{\rm tot}\}$ to label the spin states of the hexagon plaquette. From the spin composition rule for three electron spins, we have the following relation,

$$\tfrac{1}{2}\otimes\tfrac{1}{2}\otimes\tfrac{1}{2} \equiv \tfrac{1}{2}\oplus\tfrac{1}{2}\oplus\tfrac{3}{2}, \quad (9)$$

where the left-hand side is the product state of the three electron spins and the right-hand side is the total spin states $S_{\rm tot}$. For both A and B occupation configurations, there are eight spin states. Note that we have two pairs of $S_{\rm tot} = 1/2$ states for each occupation configuration.

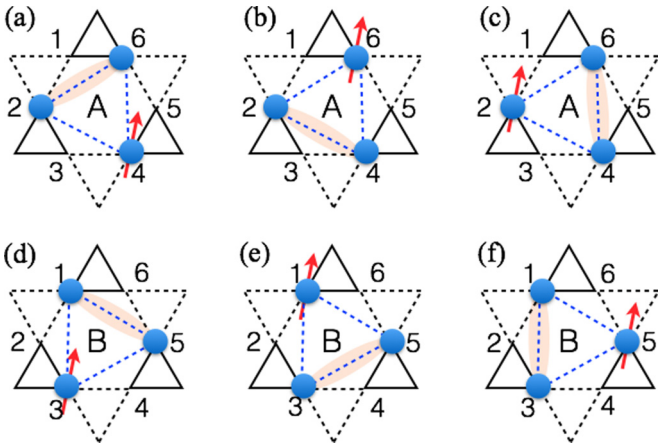

FIG. 3. Three spin-singlet positions for both A and B occupation configurations. The (orange) dimer refers to the spin singlet, and the (red) arrow is the dangling spin. The three spin-singlet configurations are related by the threefold rotation around the hexagon center.

The two states with $S_{\rm tot} = 3/2$ are simply the ferromagnetic states and are certainly not favored by the antiferromagnetic exchange interaction $H_{{\rm ex},\boldsymbol{R}}$. Directly solving the Hamiltonian $H_{\hexagon_{\boldsymbol{R}}}$, we find that when

$$J > \tfrac{2}{3}\left[K_1 + K_2 - \left(K_1^2 - K_1K_2 + K_2^2\right)^{\frac{1}{2}}\right], \qquad (10)$$

the local ground states are four symmetric states with $S_{\rm tot} = 1/2$. Here, the "symmetric" states refer to being symmetric between the A and B occupation configurations in Fig. 3. This is understood by the fact that the collective motion of three electrons favors symmetric states rather than antisymmetric ones. These fourfold degenerate states can be effectively characterized by two quantum numbers $\{s^z, \tau^z\}$ with $s^z = \pm\frac{1}{2}$ and $\tau^z = \pm\frac{1}{2}$, where s^z refers to the total spin $s^z \equiv S^z_{\rm tot} = \pm\frac{1}{2}$. The pseudospin-1/2 operator $\boldsymbol{\tau}$ refers to the emergent orbitals that will be explained below.

The wave functions of the four degenerate states are labeled by $|\tau^z s^z\rangle_{\boldsymbol{R}}$ and are given as to the order of $O(K_2/K_1)$ [33],

$$|\uparrow\uparrow\rangle_{\boldsymbol{R}} = \frac{1}{2}[|\uparrow\uparrow\downarrow\rangle_{\rm A} - |\uparrow\downarrow\uparrow\rangle_{\rm A} + |\downarrow\uparrow\uparrow\rangle_{\rm B} - |\uparrow\uparrow\downarrow\rangle_{\rm B}], \quad (11)$$

$$|\downarrow\uparrow\rangle_{\boldsymbol{R}} = \frac{\sqrt{3}}{6}[2|\downarrow\uparrow\uparrow\rangle_{\rm A} - |\uparrow\downarrow\uparrow\rangle_{\rm A} - |\uparrow\uparrow\downarrow\rangle_{\rm A} + 2|\uparrow\downarrow\uparrow\rangle_{\rm B} - |\uparrow\uparrow\downarrow\rangle_{\rm B} - |\downarrow\uparrow\uparrow\rangle_{\rm B}], \qquad (12)$$

and these other two states $|\uparrow\downarrow\rangle_{\boldsymbol{R}}, |\downarrow\downarrow\rangle_{\boldsymbol{R}}$ are simply obtained by applying a time-reversal transformation to the above two states,

$$|\uparrow\downarrow\rangle_{\boldsymbol{R}} = \frac{1}{2}[|\downarrow\downarrow\uparrow\rangle_{\rm A} - |\downarrow\uparrow\downarrow\rangle_{\rm A} + |\uparrow\downarrow\downarrow\rangle_{\rm B} - |\downarrow\downarrow\uparrow\rangle_{\rm B}], \quad (13)$$

$$|\downarrow\downarrow\rangle_{\boldsymbol{R}} = \frac{\sqrt{3}}{6}[2|\uparrow\downarrow\downarrow\rangle_{\rm A} - |\downarrow\uparrow\downarrow\rangle_{\rm A} - |\downarrow\downarrow\uparrow\rangle_{\rm A} + 2|\downarrow\uparrow\downarrow\rangle_{\rm B} - |\downarrow\downarrow\uparrow\rangle_{\rm B} - |\uparrow\downarrow\downarrow\rangle_{\rm B}]. \qquad (14)$$

We clarify the physical origin of the fourfold degeneracy of the above four states for the hexagon plaquette. First, the twofold degeneracy of $s^z = \pm 1/2$ is simply protected by time-reversal symmetry. The remaining twofold degeneracy comes from the point group symmetry of the resonating hexagon. This is ready for us to see if we can fix the occupation configuration of the three electrons. To be more specific, let us start with the A configuration in the upper panel of Fig. 3. To optimize the antiferromagnetic exchange interaction, two electron spins out of the three must form a spin singlet, leaving the third electron as a dangling spin. As shown in Fig. 3, the spin singlet can be formed between any pair of electrons, and the different arrangements of the spin singlet are related by the threefold rotation. Although there seems to be three possible singlet arrangements, only two of them are linearly independent and are responsible for the twofold degeneracy. Likewise, for the B configuration on the lower panel of Fig. 3, we again have two such degenerate states. When the three electrons start to move collectively within the hexagon between the A and B configurations, the corresponding states start to hybridize and the symmetric states are favored energetically. The twofold degeneracy survives and is given as the $\tau^z = \uparrow, \downarrow$ states in Eqs. (11)–(14).

The three electrons are localized on the resonating hexagon but are delocalized within the resonating hexagon. It is hard for them to move out of the resonating hexagon, but easy for them to move within the resonating hexagon. Due to this collective motion, the wave functions of $|\tau^z s^z\rangle$ are extended and span across the resonating hexagon, and the $\tau^z = \uparrow, \downarrow$ states behave as two degenerate orbitals that are defined on the resonating hexagon. Since the degeneracy of $\tau^z = \uparrow, \downarrow$ states originates from the arrangements of the spin singlets, the pseudospin $\boldsymbol{\tau}$ is *even* under the time-reversal transformation. The two emergent orbital states that are defined in Eqs. (11) and (12) comprise the two-dimensional E-type irreducible representation of the point group, and thus their twofold degeneracy is protected by the point group symmetry of the resonating hexagon.

IV. THE KUGEL-KHOMSKII SPIN-ORBITAL INTERACTION

In this section we study and derive the interaction between the spins and the emergent orbitals that live on the neighboring resonating hexagons. This interaction is necessarily of the Kugel-Khomskii type. Based on the Kugel-Khomskii model, we obtain the Curie-Weiss temperature and Curie constant in the strong plaquette ordered regime, and compare with the high-temperature results.

A. The Kugel-Khomskii model

The neighboring resonating hexagons are connected by a "bowtie" structure that is composed of corner-shared up and down triangles (see Fig. 4). The local moment interaction comes from the remaining exchange interaction between the two electron spins that reside on the four exterior vertices of the bowtie. To illustrate the idea, we consider the bowtie structure that connects the two resonating hexagons centered at $\boldsymbol{R}$ and $\boldsymbol{R} + \boldsymbol{a}_1$ (see Figs. 1 and 4). To derive the local moment interaction, we need to project the remaining electron spin exchange interaction onto the fourfold degenerate local moment states $|\tau^z s^z\rangle$ of each resonating hexagon. For this purpose, we first write down the interhexagon exchange interaction between the

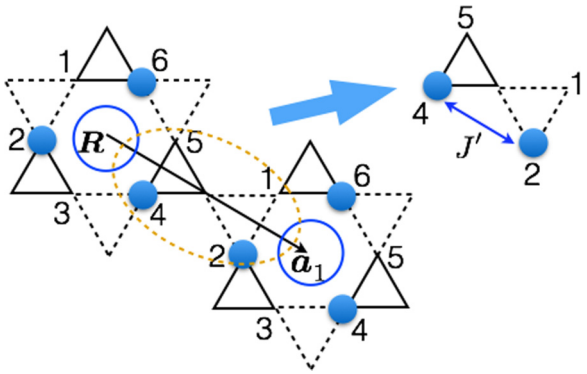

FIG. 4. The bowtie structure that connects two neighboring resonating hexagons. In the upper right-hand corner, we indicate the exchange interaction J' between two electrons.

electrons at the bowtie vertices,

$$H'_{\rm ex} = -\frac{J'}{4}[n_4(\boldsymbol{R}) + n_5(\boldsymbol{R})][n_1(\boldsymbol{R}+\boldsymbol{a}_1) + n_2(\boldsymbol{R}+\boldsymbol{a}_1)] + J'[\boldsymbol{S}_4(\boldsymbol{R})n_4(\boldsymbol{R}) + \boldsymbol{S}_5(\boldsymbol{R})n_5(\boldsymbol{R})]\cdot[\boldsymbol{S}_1(\boldsymbol{R}+\boldsymbol{a}_1) \times n_1(\boldsymbol{R}+\boldsymbol{a}_1) + \boldsymbol{S}_2(\boldsymbol{R}+\boldsymbol{a}_1)n_2(\boldsymbol{R}+\boldsymbol{a}_1)], \quad (15)$$

where we have included the exchange interactions for electrons at all four pairs of the external vertices. Again, since the position of the electron is not fixed, the electron number operator n_i is introduced. The exchange paths all go through the central vertex of the bowtie and are of equal length. Therefore, only one exchange coupling J' is introduced for all four pairs in Eq. (15). The exchange coupling J' can be obtained from the fourth-order perturbation theory and is given as

$$J' = \frac{4t_1^2t_2^2}{UV_1^2} + \frac{4t_1^2t_2^2}{UV_2^2} + \frac{4t_1^2t_2^2}{UV_1V_2}, \quad (16)$$

and the fifth-order perturbation theory could introduce more terms to J' without invoking double electron occupancy on a single lattice site. Moreover, since J' is the exchange coupling between the spins in the strong plaquette ordered regime, J' is expected to be weaker than the intraresonating-hexagon exchange coupling J in Eq. (6).

We project $H'_{\rm ex}$ onto the local ground-state manifold at resonating hexagon sites $\boldsymbol{R}$ and $\boldsymbol{R}+\boldsymbol{a}_1$ and then express the resulting interaction in terms of the spin $\boldsymbol{s}$ and the pseudospin $\boldsymbol{\tau}$. The effective interaction on other bonds can be obtained likewise. The final local moment interaction reduces to a Kugel-Khomskii model [30] that is defined on the triangular lattice formed by the resonating hexagons. To the order of $O(K_2/K_1)$, the Kugel-Khomskii model is given as

$$H_{\rm KK} = \frac{J'}{9}\sum_{\boldsymbol{R}}\sum_{\mu=x,y,z}(\boldsymbol{s}_{\boldsymbol{R}}\cdot\boldsymbol{s}_{\boldsymbol{R}+\boldsymbol{a}_\mu})[1+4T^\mu_{\boldsymbol{R}}][1-2T^\mu_{\boldsymbol{R}+\boldsymbol{a}_\mu}], \quad (17)$$

where the new set of pseudospin operators T^μ's are defined as

$$T^x_{\boldsymbol{R}} = -\frac{1}{2}\tau^z_{\boldsymbol{R}} - \frac{\sqrt{3}}{2}\tau^x_{\boldsymbol{R}}, \quad (18)$$

$$T^y_{\boldsymbol{R}} = -\frac{1}{2}\tau^z_{\boldsymbol{R}} + \frac{\sqrt{3}}{2}\tau^x_{\boldsymbol{R}}, \quad (19)$$

$$T^z_{\boldsymbol{R}} = \tau^z_{\boldsymbol{R}}, \quad (20)$$

and $\boldsymbol{a}_x = \boldsymbol{a}_1$, $\boldsymbol{a}_y = \boldsymbol{a}_2$, and $\boldsymbol{a}_z = -\boldsymbol{a}_1 - \boldsymbol{a}_2$. The particular expression of the Kugel-Khomskii model in Eq. (17) originates from the choice of two orbital wave functions in Eqs. (11)–(14). If a different set of orbital wave functions is chosen, the resulting Kugel-Khomskii model would have a different form. In Eq. (17), the effective exchange coupling is significantly reduced after the projection compared to the original exchange coupling J' in Eq. (15). The important factor 1/9 in front of this equation can be understood physically as coming from the fact that each spin is found in the bowtie structure connecting two hexagons only 1/3 of the time.

B. The Curie-Weiss laws

Since the pseudospin $\boldsymbol{\tau}$ is even under the time-reversal transformation and thus does not couple to the external magnetic field, the low-temperature Curie-Weiss temperature thus detects the spin-spin interaction, and from the Kugel-Khomskii model $H_{\rm KK}$ we directly compute the Curie constant $\mathcal{C}$ and the Curie-Weiss temperature $\Theta_{\rm CW}$ at low temperature,

$$\mathcal{C}^{\rm L} = \frac{g^2\mu_{\rm B}^2 s(s+1)}{3k_{\rm B}}\frac{N}{3}, \quad (21)$$

$$\Theta^{\rm L}_{\rm CW} = -\frac{2s(s+1)J'}{9}, \quad (22)$$

where N is the total number of electrons, g is the Landé factor, and $N/3$ in $\mathcal{C}^{\rm L}$ means the active spin degrees of freedom in the strong plaquette ordered phase comprise 1/3 of the total number of electrons. This is a natural consequence due to the spin state reconstruction within each resonating hexagon. This result is consistent with the low-temperature magnetic susceptibility $LiZn_2Mo_3O_8$ [21–24].

To make a comparison with the high-temperature susceptibility, we consider the high-temperature regime where the plaquette charge order is present and the spin singlet within the resonating hexagon plaquette is thermally destroyed. In this regime, all the electron spins contribute to the magnetic susceptibility. Therefore, the Curie constant for this high-temperature regime is simply given by

$$\mathcal{C}^{\rm H} = \frac{g^2\mu_{\rm B}^2 s(s+1)}{3k_{\rm B}}N, \quad (23)$$

and is three times larger than the low-temperature one. Moreover, in this regime, Fig. 1 is a typical electron configuration. For each electron, there are four neighboring electrons that interact with this electron spin with the pairwise spin interaction across the bowtie structure. Among these interactions, there are two intraresonating-hexagon interactions with the coupling J and two inter-resonating-hexagon interactions J'. Then the Curie-Weiss temperature for this high-temperature regime is given as

$$\Theta^{\rm H}_{\rm CW} = -\frac{2s(s+1)}{3}(J+J'), \quad (24)$$

and is $3(1+J/J')$ times larger than the low-temperature one. Since J' is expected to be less than J, the ratio is larger than 6 and provides a separation of scale between the high-temperature freezing of 2/3 of the spins and the interaction among the remaining spins. In the experiment on $LiZn_2Mo_3O_8$, the two Curie-Weiss temperatures are -220 and -14 K, respectively [23].

V. PARTON CONSTRUCTION FOR THE CANDIDATE SPIN-LIQUID STATE

As any other spin-orbital exchange model [30], the Kugel-Khomskii model $H_{\rm KK}$ in our context involves the spin-spin interaction, the pseudospin-pseudospin interaction, and the spin-pseudospin interaction, and all these interactions are of the same energy scale. These interactions together make the model analytically intractable. In the absence of the spin-pseudospin interaction, the Heisenberg spin exchange model would favor the conventional 120° state with a long-range order. The spin-pseudospin interaction, however, competes with the Heisenberg term, destabilizes the conventional 120° state, and may potentially induce a spin-liquid state. This is because the quarticlike spin-pseudospin interaction allows the local moment to fluctuate more effectively in the spin-pseudospin space. Such a spin liquid, if it exists, may be smoothly connected to the $U(1)$ spin liquid with spinon Fermi surfaces that was proposed for the weak plaquette charge ordered regime in Ref. [6].

From the experimental side, a broad continuous excitation has been discovered in the inelastic neutron scattering measurement on powder samples. The authors of Ref. [21] proposed a gapless spin-liquid state. Moreover, the neutron spectral weight in the experiment is not suppressed at low energies, which indicates that the ground state cannot be a Dirac spin liquid. Based on the experimental results, we here propose a candidate ground state to a spin liquid with a spinon Fermi surface. This phenomenological proposal is again consistent with the previous suggestion from the weak-coupling approach [6]. To demonstrate the phenomenological consequence of this proposal, we develop a parton construction that is designed for our spin-orbital model and suggest the experimental consequence of this candidate state.

A. The parton construction

There are both spin and orbital degrees of freedom on a single site $\boldsymbol{R}$. To account for both of them, we introduce the following fermionic parton representation,

$$\boldsymbol{\tau}_{\boldsymbol{R}} = \sum_{m,n}\sum_{\alpha}\frac{1}{2} f^{\dagger}_{\boldsymbol{R}m\alpha}\boldsymbol{\sigma}_{mn} f_{\boldsymbol{R}n\alpha}, \tag{25}$$

$$\boldsymbol{s}_{\boldsymbol{R}} = \sum_{m}\sum_{\alpha,\beta}\frac{1}{2} f^{\dagger}_{\boldsymbol{R}m\alpha}\boldsymbol{\sigma}_{\alpha\beta} f_{\boldsymbol{R}m\beta}, \tag{26}$$

where $m,n = \uparrow,\downarrow$ refer to the pseudospin state for the orbitals, $\alpha,\beta = \uparrow,\downarrow$ refer to the spin state, and $\boldsymbol{\sigma} = (\sigma^x,\sigma^y,\sigma^z)$ is the vector of Pauli matrices. To get back to the physical Hilbert space, we further impose a Hilbert space constraint,

$$\sum_{\alpha}\sum_{m} f^{\dagger}_{\boldsymbol{R}m\alpha} f_{\boldsymbol{R}m\alpha} = 1. \tag{27}$$

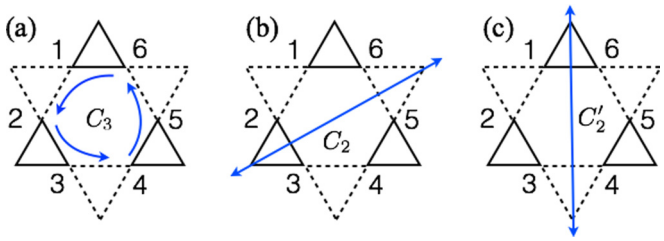

FIG. 5. (a) Threefold rotation around the center of the plaquette. (b) The twofold rotation axis. (c) Another twofold rotation axis.

Unlike the pure spin model, our spinon carries an extra orbital index. This parton construction could be well extended to other spin-orbital models.

B. The symmetry property of the spinons

A $U(1)$ spin liquid with spinon Fermi surfaces was proposed for the weak plaquette charge ordered regime [6]. For this state, the spinon transforms identically as an electron under the lattice transformation, and there is no projective realization of the lattice symmetry. Since we suggest that the possible spin liquid for our Kugel-Khomskii model in the strong-coupling regime is connected to the ground state in the weak plaquette ordered regime, we here explicitly derive the symmetry transformation of the spinons in our context.

Let us consider a single plaquette at $\boldsymbol{R}$, where the symmetries include a threefold rotation C_3 and two twofold rotations C_2 and C_2' (see Fig. 5). The lattice symmetry does not change the spin component, but acts on the orbital degree of freedom. Under C_3, the lattice sites within the hexagon plaquette transform as

$$C_3: \quad 2\to 4,\ 4\to 6,\ 6\to 2, \tag{28}$$

$$C_3: \quad 1\to 3,\ 3\to 5,\ 5\to 1, \tag{29}$$

therefore, from the orbital wave functions, we have that the states $|\uparrow\uparrow\rangle_{\boldsymbol{R}}$ and $|\downarrow\uparrow\rangle_{\boldsymbol{R}}$ transform as

$$C_3: \quad |\uparrow\uparrow\rangle_{\boldsymbol{R}} \to -\frac{1}{2}|\uparrow\uparrow\rangle_{\boldsymbol{R}} + \frac{\sqrt{3}}{2}|\downarrow\uparrow\rangle_{\boldsymbol{R}}, \tag{30}$$

$$C_3: \quad |\downarrow\uparrow\rangle_{\boldsymbol{R}} \to -\frac{\sqrt{3}}{2}|\uparrow\uparrow\rangle_{\boldsymbol{R}} - \frac{1}{2}|\downarrow\uparrow\rangle_{\boldsymbol{R}}, \tag{31}$$

where the transformation does not depend on the spin quantum number, and identical transformations are obtained for the states $|\uparrow\downarrow\rangle_{\boldsymbol{R}}$ and $|\downarrow\downarrow\rangle_{\boldsymbol{R}}$. One then establishes

$$C_3: \quad f_{\boldsymbol{R}\uparrow\alpha} \to -\frac{1}{2} f_{\boldsymbol{R}\uparrow\alpha} + \frac{\sqrt{3}}{2} f_{\boldsymbol{R}\downarrow\alpha}, \tag{32}$$

$$C_3: \quad f_{\boldsymbol{R}\downarrow\alpha} \to -\frac{\sqrt{3}}{2} f_{\boldsymbol{R}\uparrow\alpha} - \frac{1}{2} f_{\boldsymbol{R}\downarrow\alpha}. \tag{33}$$

Following the same type of calculation, under C_2 and C_2', we have

$$C_2: \quad 5\leftrightarrow 6,\ 1\leftrightarrow 4,\ 2\leftrightarrow 3, \tag{34}$$

$$C_2: \quad f_{\boldsymbol{R}\uparrow\alpha} \to -f_{\boldsymbol{R}\uparrow\alpha}, \tag{35}$$

$$C_2: \quad f_{\boldsymbol{R}\downarrow\alpha} \to +f_{\boldsymbol{R}\downarrow\alpha}, \tag{36}$$

$$C_2': \quad 1\leftrightarrow 6,\ 2\leftrightarrow 5,\ 3\leftrightarrow 4, \tag{37}$$

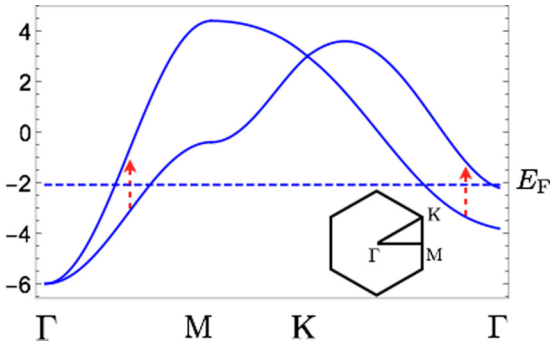

FIG. 6. The two spinon bands and their vertical particle-hole transition between the two bands. In the plot, $\tilde{t}_2 = 0.3\tilde{t}_1$, and $\tilde{t}_1 = 1$ is used as the energy unit. The inset is the Brillouin zone of the triangular lattice formed by the resonating hexagons.

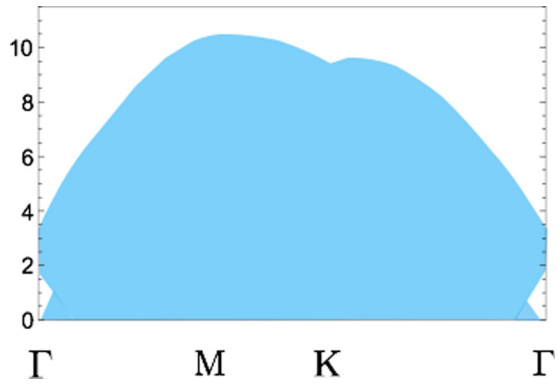

FIG. 7. The spinon continuum contribution to the spin-spin correlation function as measured by neutron scattering along the high-symmetry momentum direction. Due to the interband transition, a spinon continuum exists up to finite energies near the Γ point, with a small region of missing weight. The energy parameters here are the same as the ones in Fig. 6.

and

$$C_2': \quad f_{\boldsymbol{R}\uparrow\alpha} \to +\frac{1}{2} f_{\boldsymbol{R}\uparrow\alpha} - \frac{\sqrt{3}}{2} f_{\boldsymbol{R}\downarrow\alpha}, \tag{38}$$

$$C_2': \quad f_{\boldsymbol{R}\downarrow\alpha} \to -\frac{\sqrt{3}}{2} f_{\boldsymbol{R}\uparrow\alpha} - \frac{1}{2} f_{\boldsymbol{R}\downarrow\alpha}. \tag{39}$$

C. The spinon Fermi-surface state

From the spinon symmetry properties, we determine the generic symmetry allowed spinon mean-field Hamiltonian H_{spinon},

$$H_{\text{spinon}} = \sum_{\boldsymbol{R},\mu} \sum_{m,n} \sum_{\alpha} t^{\mu}_{mn} f^{\dagger}_{\boldsymbol{R}m\alpha} f_{\boldsymbol{R}+\boldsymbol{a}_\mu,n,\alpha} + \text{H.c.}, \tag{40}$$

where t^{μ}_{mn} is a bond-dependent hopping matrix for the spinons, and we have the symmetry allowed hoppings as

$$t^x = -\tilde{t}_1 \mathbb{1}_{2\times 2} + \tilde{t}_2 \sigma^z + \sqrt{3}\tilde{t}_2 \sigma^x, \tag{41}$$

$$t^y = -\tilde{t}_1 \mathbb{1}_{2\times 2} + \tilde{t}_2 \sigma^z - \sqrt{3}\tilde{t}_2 \sigma^x, \tag{42}$$

$$t^z = -\tilde{t}_1 \mathbb{1}_{2\times 2} - 2\tilde{t}_2 \sigma^z, \tag{43}$$

and $\mathbb{1}_{2\times 2}$ is a 2×2 identity matrix. This model describes the spinon hopping on a triangular lattice with two orbitals at each lattice site. Since the spinons are at 1/4 filling, each band is partially filled and the system develops spinon Fermi surfaces (see Fig. 6). The mean-field ground state is obtained by filling the spinon states below the Fermi energy E_F,

$$|\Psi_{\text{MF}}\rangle = \prod_{E_{\boldsymbol{k},j} < E_F} \xi^{\dagger}_{\boldsymbol{k}j\uparrow} \xi^{\dagger}_{\boldsymbol{k}j\downarrow} |0\rangle, \tag{44}$$

where $E_{\boldsymbol{k},j}$ is the energy of the eigenmode that is defined by $\xi^{\dagger}_{\boldsymbol{k}j\uparrow}$ or $\xi^{\dagger}_{\boldsymbol{k}j\downarrow}$, and is given as

$$E_{\boldsymbol{k},1} = -2\tilde{t}_1(c_x + c_y + c_z) + 4|\tilde{t}_2|\big(c_x^2 + c_y^2 + c_z^2 - c_y c_z - c_x c_z - c_x c_y\big)^{\frac{1}{2}}, \tag{45}$$

$$E_{\boldsymbol{k},2} = -2\tilde{t}_1(c_x + c_y + c_z) - 4|\tilde{t}_2|\big(c_x^2 + c_y^2 + c_z^2 - c_y c_z - c_x c_z - c_x c_y\big)^{\frac{1}{2}}. \tag{46}$$

Here, $c_\mu = \cos(\boldsymbol{k} \cdot \boldsymbol{a}_\mu)$.

D. The qualitative feature of the spinon continuum due to the emergent orbitals

The key property for the spinon mean-field model is the presence of the interorbital hopping $\tilde{t}_2$ that hybridizes different orbitals such that each spinon band no longer has a definite orbital character. This interorbital spinon hopping arises from the fact that the orbital interaction is anisotropic in the orbital space and only respects the discrete lattice symmetry. In inelastic neutron scattering, the neutron would only see the effective spin and not see the emergent orbital degree of freedom. The orbital degree of freedom, however, has an important effect on the spinon continuum that is observed by inelastic neutron scattering. The neutron detects the particle-hole excitation across the spinon Fermi level. From the momentum and energy conservation, we have the momentum and energy transfer of the neutron as

$$\boldsymbol{q} = \boldsymbol{q}_1 - \boldsymbol{q}_2, \tag{47}$$

$$E = E_{\boldsymbol{q}_1,j_1} - E_{\boldsymbol{q}_2,j_2}, \tag{48}$$

where $\boldsymbol{q}_1$ and $E_{\boldsymbol{q}_1,j_1}$ are the momentum and the energy of an unoccupied spinon while $\boldsymbol{q}_2$ and $E_{\boldsymbol{q}_2,j_2}$ are the momentum and the energy of the filled spinon. The particle-hole excitation would involve both the intraband transitions (with $j_1 = j_2$) and the interband transitions (with $j_1 \neq j_2$). If there is no orbital degree of freedom and there is only one single spinon band, the interband transition is not involved, and the inelastic neutron scattering spectral weight for the intraband transition is suppressed for the finite energies at the Γ point. This is because at the mean-field level the intraband process always excites the finite-energy spinon particle-hole pair with a finite momentum. In contrast, with the interband vertical process (see

Fig. 6), the spinon particle-hole pair with zero momentum can carry a wide range of finite energies. In Fig. 7, we explicitly compute the energy and momentum spread of the contribution to the spin-spin correlation function as measured by neutron scattering due to the spinon particle-hole pair excitation for a specific choice of spinon hoppings. Qualitatively, a broad continuum is observed, with a small amount of missing weight near the Γ point due to the features of the interband transition.

VI. EMERGENT ORBITAL ORDER IN A FIELD

Despite the possible exotic spin-liquid ground state at zero field, the Kugel-Khomskii model $H_{\rm KK}$ becomes more tractable in the presence of a strong external magnetic field. Due to the suppression of the exchange coupling in $H_{\rm KK}$, it is feasible to choose the magnetic fields to fully polarize the local spin moments such that $s^z = \uparrow$ for every resonating hexagon, but at the same time keep the field from polarizing all the electron spins in the kagome system. The pseudospin $\boldsymbol{\tau}$ is not directly effected by the magnetic field since it does not couple to the Zeeman field. The pseudospins remain active, and the interaction between them turns out to be a ferromagnetic compass model on the triangular lattice formed by the resonating hexagons,

$$H_{\rm RKK} = -\frac{2J'}{9}\sum_{\boldsymbol{R}}\sum_{\mu=x,y,z} T^{\mu}_{\boldsymbol{R}} T^{\mu}_{\boldsymbol{R}+\boldsymbol{a}_\mu}. \tag{49}$$

From a standard Luttinger-Tisza type of mean-field approach [34], we find that the mean-field ground state of $H_{\rm RKK}$ has an accidental $U(1)$ continuous degeneracy, i.e., any ferro-orbital ($\boldsymbol{q} = \boldsymbol{0}$) state with the pseudospin $\boldsymbol{\tau}$ orienting in the xz plane is a classical ground state. Here, we parametrize the mean-field pseudospin order as

$$\boldsymbol{\tau}_{\rm cl} = \tfrac{1}{2}(\cos\theta\,\hat{z} + \sin\theta\,\hat{x}), \tag{50}$$

with $\theta \in [0, 2\pi)$.

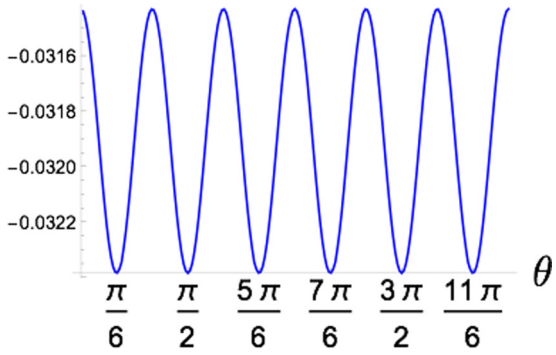

FIG. 8. The quantum zero-point energy per resonating hexagon for the mean-field orbital order. The energy unit is set to $2J'/9$ in the figure.

This continuous $U(1)$ ground-state degeneracy at the mean-field level of the reduced Kugel-Khomskii model $H_{\rm RKK}$ is lifted when the quantum fluctuations of the orbitals are included. We study this quantum order by the disorder phenomenon from the linear orbital-wave theory. Here, we introduce the Holstein-Primakoff boson to represent the pseudospin operator $\boldsymbol{\tau}_{\boldsymbol{R}}$ as follows,

$$\boldsymbol{\tau}_{\boldsymbol{R}} \cdot \hat{\boldsymbol{\tau}}_{\rm cl} = \frac{1}{2} - a^{\dagger}_{\boldsymbol{R}} a_{\boldsymbol{R}}, \tag{51}$$

$$\boldsymbol{\tau}_{\boldsymbol{R}} \cdot \hat{y} = \frac{1}{2i}[a_{\boldsymbol{R}} - a^{\dagger}_{\boldsymbol{R}}], \tag{52}$$

$$\boldsymbol{\tau}_{\boldsymbol{R}} \cdot (\hat{y} \times \hat{\boldsymbol{\tau}}_{\rm cl}) = \frac{1}{2}[a_{\boldsymbol{R}} + a^{\dagger}_{\boldsymbol{R}}], \tag{53}$$

where $\hat{\boldsymbol{\tau}}_{\rm cl} \equiv \boldsymbol{\tau}_{\rm cl}/|\boldsymbol{\tau}_{\rm cl}|$ is the orientation of the pseudospin. We keep the quadratic terms in the Holstein-Primakoff boson operators and express the reduced Kugel-Khomskii model as

$$H_{\rm RKK} = \sum_{\boldsymbol{k}\in {\rm BZ}} [2A_{\boldsymbol{k}} a^{\dagger}_{\boldsymbol{k}} a_{\boldsymbol{k}} + B_{\boldsymbol{k}}(a_{\boldsymbol{k}} a_{-\boldsymbol{k}} + {\rm H.c.})] + E_{\rm cl}, \tag{54}$$

where "BZ" refers to the Brillouin zone of the triangular lattice formed by the resonating hexagon plaquettes and

$$E_{\rm cl} = -\frac{J'}{12}\frac{N}{3}, \tag{55}$$

$$A_{\boldsymbol{k}} = \frac{2J'}{9}\left[-\frac{\sin^2(\theta-\pi/3)}{4}\cos(\boldsymbol{k}\cdot\boldsymbol{a}_x) - \frac{\sin^2(\theta+\pi/3)}{4}\cos(\boldsymbol{k}\cdot\boldsymbol{a}_y) - \frac{\sin^2\theta}{4}\cos(\boldsymbol{k}\cdot\boldsymbol{a}_z) + \frac{3}{4}\right], \tag{56}$$

$$B_{\boldsymbol{k}} = \frac{2J'}{9}\left[-\frac{\sin^2(\theta-\pi/3)}{4}\cos(\boldsymbol{k}\cdot\boldsymbol{a}_x) - \frac{\sin^2(\theta+\pi/3)}{4}\cos(\boldsymbol{k}\cdot\boldsymbol{a}_y) - \frac{\sin^2\theta}{4}\cos(\boldsymbol{k}\cdot\boldsymbol{a}_z)\right]. \tag{57}$$

The linear orbital-wave Hamiltonian is then diagonalized by a Bogoliubov transformation for the Holstein-Primakoff bosons and is given by

$$H_{\rm RKK} = E_{\rm cl} + \sum_{\boldsymbol{k}\in{\rm BZ}}\left[\frac{\omega_{\boldsymbol{k}}}{2} - A_{\boldsymbol{k}}\right] + \sum_{\boldsymbol{k}\in{\rm BZ}} \omega_{\boldsymbol{k}} \alpha^{\dagger}_{\boldsymbol{k}} \alpha_{\boldsymbol{k}},$$

where the orbital-wave (or "orbiton") mode reads

$$\omega_{\boldsymbol{k}} = 2\left(A^2_{\boldsymbol{k}} - B^2_{\boldsymbol{k}}\right)^{\frac{1}{2}}. \tag{58}$$

From Eq. (58), the quantum correction to the ground-state energy is

$$\Delta E = \sum_{\boldsymbol{k}\in{\rm BZ}}\left[\frac{\omega_{\boldsymbol{k}}}{2} - A_{\boldsymbol{k}}\right]. \tag{59}$$

In Fig. 8, we plot the quantum correction as a function of the angular parameter θ. The minima occur at

$$\theta = \frac{\pi}{6} + \frac{n\pi}{3}, \quad n \in \mathcal{Z}, \tag{60}$$

and are indicated in Fig. 9(a).

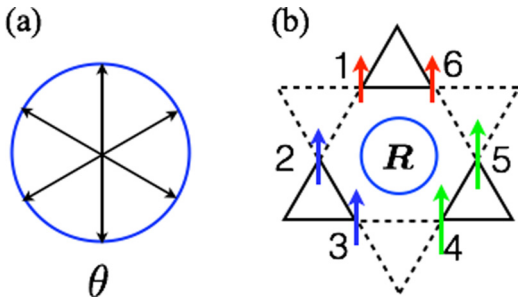

FIG. 9. (a) The selection of the θ on a unit circle by quantum fluctuation. The arrow indicates the optimal choice. (b) The magnetic moment distribution within the resonating hexagon for $\theta = \pi/6$. It is clear that the threefold rotation about the center of the hexagon is broken.

Since the twofold orbital degeneracy arises from the point group symmetry, the emergent orbital order, which breaks the orbital degeneracy, has to be related to the symmetry breaking. To understand the physical consequence of the orbital order, we consider the following product state wave function that is appropriate for the $\boldsymbol{q} = \boldsymbol{0}$ ferro-orbital state,

$$|\Psi\rangle_{\text{orb}} = \prod_{\boldsymbol{R}} \left[\cos\frac{\theta}{2}|\uparrow\uparrow\rangle_{\boldsymbol{R}} + \sin\frac{\theta}{2}|\downarrow\uparrow\rangle_{\boldsymbol{R}} \right]. \tag{61}$$

This variational wave function gives the orbital ordering in Eq. (50). From this wave function, we find that the electron density is uniform at every site within each resonating hexagon and thus preserves the rotation and reflection symmetries. We then compute the local magnetization for each site within the resonating hexagon,

$$\langle s_1^z\rangle_{\boldsymbol{R}} = \langle s_6^z\rangle_{\boldsymbol{R}} = \frac{1}{12} + \frac{\sin(\theta - \pi/6)}{6}, \tag{62}$$

$$\langle s_2^z\rangle_{\boldsymbol{R}} = \langle s_3^z\rangle_{\boldsymbol{R}} = \frac{1}{12} + \frac{\sin\theta}{6}, \tag{63}$$

$$\langle s_4^z\rangle_{\boldsymbol{R}} = \langle s_5^z\rangle_{\boldsymbol{R}} = \frac{1}{12} - \frac{\sin(\theta + \pi/6)}{6}. \tag{64}$$

Although the total local magnetization of each resonating hexagon is $\langle s^z\rangle_{\boldsymbol{R}} = \sum_{i=1}^{6}\langle s_i^z\rangle_{\boldsymbol{R}} = 1/2$, the orbital ordering leads to a modulation of the spin ordering inside each resonating hexagon [see Fig. 9(b)]. The threefold rotational symmetry about the center of the resonating hexagon is explicitly broken by the orbital ordering.

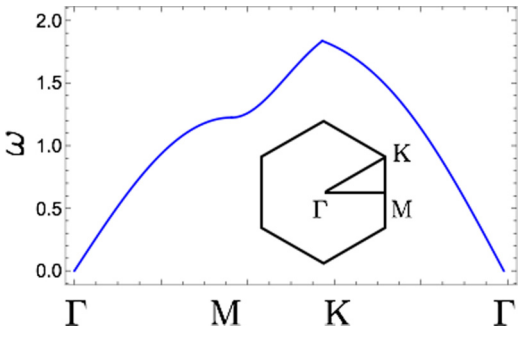

FIG. 10. The orbiton dispersion along the high-symmetry momentum line. The inset is the Brillouin zone of the triangular lattice formed by the resonating hexagons. The energy unit is set to $2J'/9$ in the figure.

In Fig. 10, we plot the dispersion of the orbiton excitation for $\theta = \pi/6$. We find the dispersion is gapless at the Γ point due to the breaking of the accidental $U(1)$ degeneracy. This pseudo-Goldstone mode is expected to be gapped if the interaction between the Holstein-Primakoff bosons is included. Since the interaction-induced gap should be very small compared to the orbiton energy scale, one would expect to observe the heat capacity $C_v \sim T^2$ at low temperatures.

VII. DISCUSSION

We discuss the experimental consequences of the plaquette charge order, the emergent orbitals, and the orbital orders. The plaquette charge order explicitly breaks the lattice translation symmetry and would lead to some variation of the bond lengths according to the symmetry breaking. This may be detected by high-resolution x-ray scattering or x-ray pair distribution function (PDF) measurements. The plaquette charge order reconstructs the spin states within each resonant hexagon leading to the freezing of 2/3 of the spins, as observed in the spin susceptibility in $LiZn_2Mo_3O_8$ [21–25]. A different explanation for the susceptibility anomaly in $LiZn_2Mo_3O_8$ based on the lattice distortion and the emergent lattices has been proposed in a previous work [26]. Both this previous work and the current work require a translation symmetry breaking by tripling the crystal unit cell. Such a translation symmetry breaking has not yet been observed in the experiment. Here, we point out the possible reason, namely, that under certain conditions, the symmetry breaking must be short ranged at all temperatures.

The Li ion is mobile and may make the system slightly off stoichiometric. To accommodate the missing or extra charges, the system needs to create domain walls within the symmetry-broken phase. An example of such domain walls is shown in Fig. 11 for the case when the filling is slightly more than 1/6. Each solid dot represents the charge order shown in Fig. 1. Note that the charge order can be centered on one of three hexagons, thereby forming ABC-type domains. A certain density of domain walls will be required for a given deviation from 1/6 filling. There is an energy cost per unit length of the domain wall, because electrons are now forced to occupy neighboring sites. The resulting state is expected to be a "liquid" state with an exponential decay of correlations for the electron charge density [27]. This result is special for the hexagonal arrangement of domain walls and the reason is as follows. It was pointed out by Villain [35] that there exists a breathing mode that expands or shrinks one particular domain but costs no energy because the total domain wall length is not changed. This is illustrated in Fig. 12. Consequently, the free energy of the system of domain walls is purely entropic and is proportional to temperature T. In the long-wavelength limit, the elastic constant of the system is also proportional to T and so is the energy to create a dislocation. An example of a dislocation is shown in Fig. 13. By the usual Berezinskii-Kosterlitz-Thouless (BKT) argument, the competition of this energy with the entropy associated with the dislocation determines whether the dislocation will

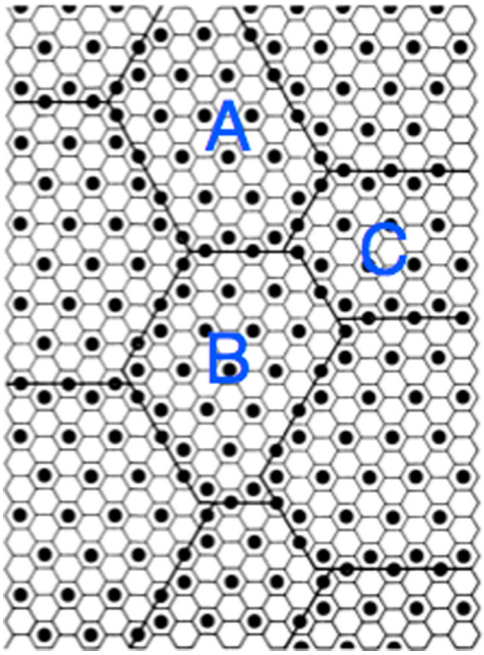

FIG. 11. A picture of the domain walls separating the ABC domains when the electron occupation is off stoichiometric, in this case slightly more than 1/6 per Mo.

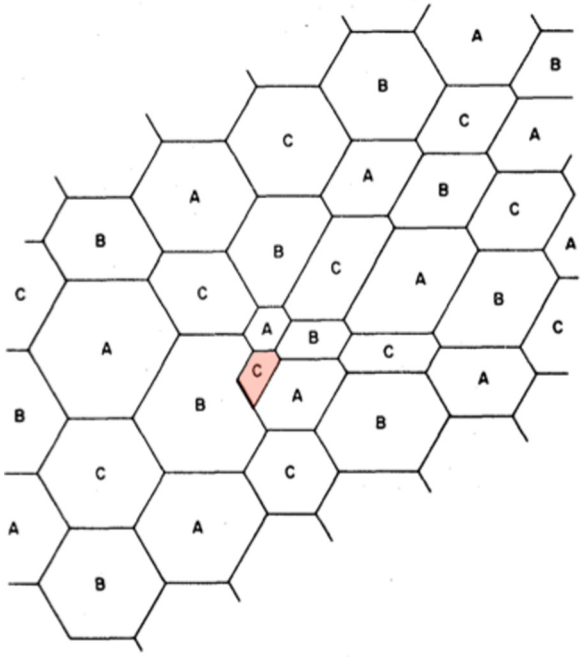

FIG. 13. A picture of a dislocation center (in red) in the system of domain walls.

proliferate, resulting in an exponentially decaying correlation function. Unlike the usual BKT argument, where the dislocation energy is a constant and a phase transition is predicted at a finite temperature, here the result depends on the numerical coefficient of the linear T term in the elastic energy. A detailed computation carried out in Ref. [27] showed that the system is always disordered at any temperature. A short-range charge ordering makes detection more difficult, but not impossible. Perhaps resonant x-ray scattering which couples directly to the electrons will have a better chance of seeing this distortion.

The emergent orbital is a degree of freedom that naturally emerges from the plaquette charge order on the breathing kagome lattice. The presence of this extra degree of freedom distinguishes the current proposal from the previous one in Ref. [26]. However, the emergent orbital is not detectable in the magnetization measurement since the orbital does not couple directly to the external magnetic field. However, it does contribute to the heat capacity and the entropy. We expect an additional entropy from the emergent orbitals apart from the spin entropy. The suggested spinon Fermi surface ground state and the spinon excitation should be detectable via inelastic neutron scattering. In fact, the existing measurement does suggest a broad continuum of excitations [21], even though the measurement was taken on powder samples. Since the qualitative feature for the spinon interband particle-hole excitation is more visible at the Γ point, optical measurements or Raman scattering can be useful for detecting the finite-energy spinon continuum at the Γ point.

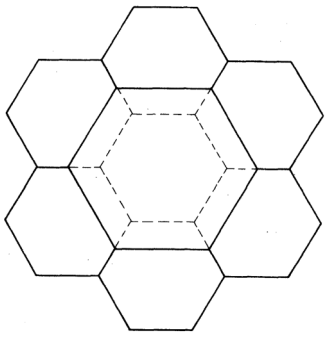

FIG. 12. The breathing mode of Villain [35]. Note that the total wall length and hence its energy has not changed. This mode contributes only to the entropy.

A magnetic field that is of the order of the low-temperature Curie-Weiss temperature is expected to polarize the spin degree of freedom. The magnetic field should be much less than the high-temperature Curie-Weiss temperature to prevent polarizing the spins that form the spin singlet within the resonating hexagon. The remaining orbital degrees of freedom then develop an orbital order via a quantum order by disorder mechanism and support a pseudo-Goldstone mode that gives a heat capacity $C_v \sim T^2$ at low temperatures. The orbital wave excitation may be detected by resonant inelastic x-ray scattering. The orbital order creates a magnetic moment redistribution within the resonating hexagon. This intrahexagon static magnetic structure may be detected by high-resolution neutron scattering, muon spin rotation (μSR), and/or NMR measurements.

Finally, there exists a large family of cluster magnets in which the electrons are localized on the cluster units and form CMIs [5–13,19,20]. The physical properties of many of these cluster magnets have not been explored carefully. Recently, $1T$-TaS_2 was proposed as a spin-liquid candidate [12]. In this system, the low-temperature (commensurate) charge density wave order enlarges the unit cell such that there exists one

localized and unpaired electron inside the 13-site star-of-David cluster. This system can thus be considered as a CMI [12]. These clustered localized electrons form effective spin-1/2 local moments that interact with each other and may develop a spin-liquid ground state [12]. Besides these two-dimensional cluster magnets, Ta-based and Mo-based lacunar spinels are good examples of three-dimensional CMIs [5,9–11]. In these materials, the systems naturally host a breathing pyrochlore lattice structure where one half of the tetrahedral clusters is smaller than the other half and host the localized electrons [5]. The study on these systems is quite limited so far. We expect that the cluster localization of the electrons in these CMIs may bring some interesting phenomena and enrich our understanding of Mott physics.

ACKNOWLEDGMENTS

G.C. is supported by the Ministry of Science and Technology of China Grant No. 2016YFA0301001, the Research Initiative Funds and the Program of First-Class University Construction of Fudan University, and the Thousand-Youth-Talent Program of China. P.A.L. is supported by the U.S. National Science Foundation under Contract No. DMR-1522575. G.C. was also supported by NSF-PHY11-25915.

[1] W. Witczak-Krempa, G. Chen, Y. B. Kim, and L. Balents, Correlated quantum phenomena in the strong spin-orbit regime, Annu. Rev. Condens. Matter Phys. **5**, 57 (2014).

[2] S. Maekawa, T. Tohyama, S. E. Barnes, S. Ishihara, W. Koshibae, and G. Khaliullin, *Physics of Transition Metal Oxides*, Springer Series in Solid-State Sciences (Springer, Berlin, 2004).

[3] Y. Tokura and N. Nagaosa, Orbital physics in transition-metal oxides, Science **288**, 462 (2000).

[4] G. Khaliullin, Orbital order and fluctuations in Mott insulators, Prog. Theor. Phys. Suppl. **160**, 155 (2005).

[5] G. Chen, H.-Y. Kee, and Y. B. Kim, Fractionalized Charge Excitations in a Spin Liquid on Partially Filled Pyrochlore Lattices, Phys. Rev. Lett. **113**, 197202 (2014).

[6] G. Chen, H.-Y. Kee, and Y. B. Kim, Cluster Mott insulators and two Curie-Weiss regimes on an anisotropic kagome lattice, Phys. Rev. B **93**, 245134 (2016).

[7] J.-P. Lv, G. Chen, Y. Deng, and Z. Y. Meng, Coulomb Liquid Phases of Bosonic Cluster Mott Insulators on a Pyrochlore Lattice, Phys. Rev. Lett. **115**, 037202 (2015).

[8] J. Carrasquilla, G. Chen, and R. G. Melko, Tripartite entangled plaquette state in a cluster magnet, Phys. Rev. B **96**, 054405 (2017).

[9] M. M. Abd-Elmeguid, B. Ni, D. I. Khomskii, R. Pocha, D. Johrendt, X. Wang, and K. Syassen, Transition from Mott Insulator to Superconductor in $GaNb_4Se_8$ and $GaTa_4Se_8$ under High Pressure, Phys. Rev. Lett. **93**, 126403 (2004).

[10] D. Hirai, M. Bremholm, J. M. Allred, J. Krizan, L. M. Schoop, Q. Huang, J. Tao, and R. J. Cava, Spontaneous Formation of Zigzag Chains at the Metal-Insulator Transition in the β-Pyrochlore CsW_2O_6, Phys. Rev. Lett. **110**, 166402 (2013).

[11] H.-S. Kim, J. Im, M. J. Han, and H. Jin, Spin-orbital entangled molecular j_{eff} states in lacunar spinel compounds, Nat. Commun. **5**, 3988 (2014).

[12] K. T. Law and P. A. Lee, 1T-TaS_2 as a quantum spin liquid, Proc. Natl. Acad. Sci. U.S.A. **114**, 6996 (2017).

[13] P. G. Radaelli, Y. Horibe, M. Gutmann, H. Ishibashi, C. H. Chen, R. M. Ibberson, Y. Koyama, Y.-S Hor, V. Kiryukhin, and S.-W. Cheong, Formation of isomorphic Ir^{3+} and Ir^{4+} octamers and spin dimerization in the spinel $CuIr_2S_4$, Nature (London) **416**, 155 (2002).

[14] F. Pollmann, P. Fulde, and K. Shtengel, Kinetic Ferromagnetism on a Kagome Lattice, Phys. Rev. Lett. **100**, 136404 (2008).

[15] S. V. Isakov, S. Wessel, R. G. Melko, K. Sengupta, and Y. B. Kim, Hard-Core Bosons on the Kagome Lattice: Valence-Bond Solids and Their Quantum Melting, Phys. Rev. Lett. **97**, 147202 (2006).

[16] F. Pollmann, K. Roychowdhury, C. Hotta, and K. Penc, Interplay of charge and spin fluctuations of strongly interacting electrons on the kagome lattice, Phys. Rev. B **90**, 035118 (2014).

[17] K. Ferhat and A. Ralko, Phase diagram of the $\frac{1}{3}$-filled extended Hubbard model on the kagome lattice, Phys. Rev. B **89**, 155141 (2014).

[18] A. Rüegg and G. A. Fiete, Fractionally charged topological point defects on the kagome lattice, Phys. Rev. B **83**, 165118 (2011).

[19] P. Gall, R. Al Rahal Al Orabi, T. Guizouarn, and P. Gougeon, Synthesis, crystal structure and magnetic properties of $Li_2InMo_3O_8$: A novel reduced molybdenum oxide containing magnetic Mo_3 clusters, J. Solid State Chem. **208**, 99 (2013).

[20] C. C. Torardi and R. E. McCarley, Synthesis, crystal structures, and properties of lithium zinc molybdenum oxide ($LiZn_2Mo_3O_8$), zinc molybdenum oxide ($Zn_3Mo_3O_8$), and scandium zinc molybdenum oxide ($ScZnMo_3O_8$), reduced derivatives containing the Mo_3O_{13} cluster unit, Inorg. Chem. **24**, 476 (1985).

[21] M. Mourigal, W. T. Fuhrman, J. P. Sheckelton, A. Wartelle, J. A. Rodriguez-Rivera, D. L. Abernathy, T. M. McQueen, and C. L. Broholm, Molecular Quantum Magnetism in $LiZn_2Mo_3O_8$, Phys. Rev. Lett. **112**, 027202 (2014).

[22] J. P. Sheckelton, F. R. Foronda, L. D. Pan, C. Moir, R. D. McDonald, T. Lancaster, P. J. Baker, N. P. Armitage, T. Imai, S. J. Blundell, and T. M. McQueen, Phys. Rev. B **89**, 064407 (2014).

[23] J. P. Sheckelton, J. R. Neilson, D. G. Soltan, and T. M. McQueen, Nat. Mater. **11**, 493 (2012).

[24] J. P. Sheckelton, J. R. Neilson, and T. M. McQueen, Electronic tunability of the frustrated triangular-lattice cluster magnet $LiZn_{2-x}Mo_3O_8$, Mater. Horiz. **2**, 76 (2015).

[25] A. Akbari-Sharbaf, R. Sinclair, A. Verrier, D. Ziat, H. D. Zhou, X. F. Sun, and J. A. Quilliam, Tunable quantum spin liquidity in the 1/6th-filled breathing kagome lattice, arXiv:1709.01904.

[26] R. Flint and P. A. Lee, Emergent Honeycomb Lattice in $LiZn_2Mo_3O_8$, Phys. Rev. Lett. **111**, 217201 (2013).

[27] S. N. Coppersmith, D. S. Fisher, B. I. Halperin, P. A. Lee, and W. F. Brinkman, Dislocations and the commensurate-incommensurate transition in two dimensions, Phys. Rev. B **25**, 349 (1982).

[28] O. I. Motrunich, Variational study of triangular lattice spin-1/2 model with ring exchanges and spin liquid state in $k-(ET)_2Cu_2(CN)_3$, Phys. Rev. B **72**, 045105 (2005).

[29] S.-S. Lee and P. A. Lee, U(1) Gauge Theory of the Hubbard Model: Spin Liquid States and Possible Application to $k-(BEDT-TTF)_2Cu_2(CN)_3-()2Cu2(CN)3$, Phys. Rev. Lett. **95**, 036403 (2005).

[30] K. I. Kugel and D. I. Khomskii, The Jahn-Teller effect and magnetism: transition metal compounds, Sov. Phys. Usp. **25**, 231 (1982).

[31] R. Moessner, S. L. Sondhi, and P. Chandra, Phase diagram of the hexagonal lattice quantum dimer model, Phys. Rev. B **64**, 144416 (2001).

[32] N. Read and S. Sachdev, Spin-Peierls, valence-bond solid, and Néel ground states of low-dimensional quantum antiferromagnets, Phys. Rev. B **42**, 4568 (1990).

[33] We expect that $V_1 \gtrsim V_2, t_1 > t_2$, so $K_1 \gg K_2$ for $LiZn_2Mo_3O_8$.

[34] J. M. Luttinger and L. Tisza, Theory of dipole interaction in crystals, Phys. Rev. **70**, 954 (1946).

[35] J. Villain, in *Ordering in Strongly Fluctuating Condensed Matter Systems*, edited by T. Riste (Plenum, New York, 1980), p. 221.